

Transport due to Transient Progressive Waves

Juan M. Restrepo^{1,2,†}, Jorge M. Ramírez³

¹Department of Mathematics, Oregon State University, Corvallis OR 97330 USA

²Kavli Institute of Theoretical Physics, University of California at Santa Barbara, Santa Barbara CA 93106 USA.

³Departamento de Matemáticas, Universidad Nacional de Colombia Sede Medellín, Medellín Colombia

(Received xx; revised xx; accepted xx)

We describe and analyze the mean transport due to transient progressive waves, including breaking waves. The waves are packets and are generated with a boundary-forced air-water two-phase Navier Stokes solver. The analysis is done in the Lagrangian frame. We show that the transport generated by these waves is significantly larger than the transport generated by steady waves. The numerically generated parcel paths suggest a model for the transport that is primarily driven by an irrotational approximation of the velocity. Wave breaking is shown to increase the variability in the transport. Breaking is accounted for in the transport model via an additive stochastic velocity term.

Key words: Authors should not enter keywords

1. Introduction

This work focuses on the mean transport due to transient progressive waves of small as well as large amplitude, including breaking waves. The estimate that leads to the classical Stokes drift formula relies critically on an assumption in the wave statistics that does not necessarily hold for transient waves. Hence one of the challenges in studying transport due to transient progressive waves is in defining meaningful and useful notions of global mean transport. Compounding this is the added challenge of determining how the very transient phenomena of wave breaking affects transport.

A simple yet generic type of progressive wave that exhibits complex transient behavior is a wave packet. We will show that significant transport is generated by these waves, as compared to the transport due to periodic steady waves. We will make use of a Lagrangian description of the fluid flow in order to characterize and understand the transport. The waves are generated by a forcing boundary condition. Solutions to the Navier-Stokes equations are approximated by numerical means, for a heavy fluid (water) and an overlying light fluid (air). The Lagrangian parcel paths are computed, using interpolation from the grid Eulerian velocity.

Our primary goal is to describe average transport at spatio-temporal scales larger than those typical of waves. To this end we will be applying ensemble characterizations to describe averaged transport. We will also make use of the insights gained from the analyses of parcel paths to propose a simple model for the averaged transport. The

† Email address for correspondence: restrepo@math.oregonstate.edu

numerically-generated transport considered in this paper revisits the transport results reported in Deike *et al.* (2017), hereon, DPM17. We use the same data, in fact. How mean transport due to waves affect the dynamics of oceans at time and space scales larger than waves has been the subject of considerable attention (see McWilliams & Restrepo (1999)). It is central, for example, to Langmuir turbulence (see McWilliams *et al.* (1997), Sullivan & McWilliams (2010)). How Langmuir turbulence and oceanic processes that depend critically on wave-generated transport are affected by waves with transient behavior is not known, however. Since we have the means to do so we will also consider how transport is affected by wave breaking. Wave breaking plays an important role in a variety of air-sea interactions, affecting stress conditions at the free surface, as well as chemical and biological balances and thermodynamics processes (see Melville (1996), Burchard (2001)). It also is a prominent mechanism in the dynamics of air-water chemical and biological exchanges, transport and dispersion of pollutants and phytoplankton. Wave breaking dissipates wave energy and momentum is exchanged between the waves and currents (see Restrepo *et al.* (2011)).

2. Generation of Numerical Progressive Wave Lagrangian Paths

In DPM17 the authors employ Gerris (Popinet (2009)), a Navier Stokes equation solver, to obtain approximations of the motion of an air/water fluid under the action of a downward gravity force with magnitude g . Time is denoted by t and the simulation runs until $t = T_f = 35$ s. The computations are done in two space dimensions with transverse coordinate denoted by x and z as the vertical coordinate which increases upward from the quiescent reference level, $z = 0$. The ‘tank’ extent is 24m, and the depth h , of the water-filled tank is 1m. The air/water interface has surface tension. The fluid is subjected to a time dependent ‘paddle’ forcing boundary condition at $x = 0$, generating a wave packet which dissipates at the beach end of the tank where absorbing boundary conditions are specified. Zero velocity boundary conditions are imposed at the bottom of the tank, $z = -h$, and at $z = h$, the top of the domain. The Navier Stokes solver uses the fresh water and air kinematic viscosity ratio and the computations reach Reynolds numbers in the order of 40,000 (The details of the numerical generation of the flow are found in DPM17). At rest, initial conditions are invoked in all of the numerical simulations. The Eulerian velocity is denoted by $\mathbf{q}(x, z, t)$, and the free surface is $z = \eta(x, t)$.

An irrotational and incompressible solution for the free surface and the velocity in the fluid domain, for infinitesimal waves are, respectively,

$$\begin{aligned}\eta(x, t) &= \sum_{n=1}^N a_n \cos(k_n(x - x_b) - \omega_n t), \\ \mathbf{u}^w(x, z, t) &= \nabla \phi(x, z, t), \quad \text{where} \\ \phi &= - \sum_{n=1}^N \frac{a_n \omega_n}{k_n} \frac{\cosh(k_n(z + h))}{\sinh(k_n h)} \sin(k_n(x - x_b) - \omega_n t),\end{aligned}\tag{2.1}$$

where $x_b = 12$ m, $t_b = 25$ s are respectively, the focusing position and time, and $t \geq 0$. In the simulations, $N = 32$. This solution, which we will connote as the *linear* wave solution, was used to generate the forcing boundary conditions for the paddle: The paddle was prescribed by the above linear wave solution (2.1), setting $x = 0$. The dispersion relation relates the angular frequencies $\omega_n = \sqrt{g k_n \tanh(k_n h)}$, to the k_n wavenumbers. The amplitudes a_n were prescribed as follows: They introduce the *slope* S , a parameter in the simulations. $S = \sum_{n=1}^N k_n a_n = Ns$, and $s = k_n a_n$, constant, $n = 0, 1, \dots, N - 1$.

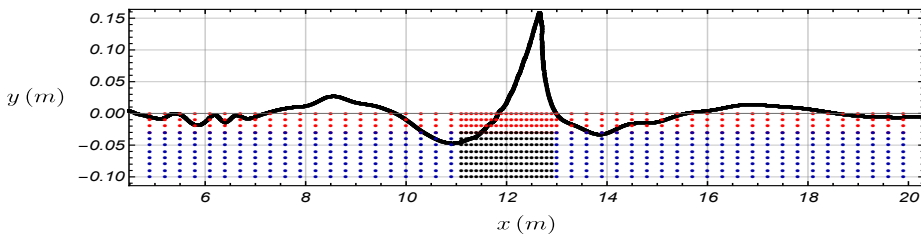


FIGURE 1. Detail of tank. The dots indicate initial positions $\mathbf{Z}(0)$ of parcel paths used in the analysis. The free surface of the wave right before breaking is shown, for the case $S = 0.38$. Points in red generate ‘surface’ paths. In black are points $|X(0) - x_b| < \frac{\lambda}{2}$. These are taken as realizations of the same random event. In green are all other paths considered.

In the specification of each run the slope $S \in [0.16, 0.4]$ is fixed, and serves as the ordering parameter. The wavenumbers k_n were found using the dispersion relation and the frequencies chosen as follows: The component frequencies $\nu_n = 0.5458 + n\delta_\nu$ Hz, where $\delta_\nu = 0.0222$ Hz. The central frequency is denoted $\nu_c = \omega_c/2\pi = 0.89$ Hz. Parcel paths $\mathbf{Z}(t) = (X(t), Z(t))$ were computed by an explicit first order in time tracer advection scheme using the velocity field from the Navier-Stokes solver, using second-order interpolation. The numerics approximately solve the parcel path equation

$$\dot{\mathbf{Z}}(t) = \mathbf{q}(\mathbf{Z}(t), t). \quad (2.2)$$

Figure 1 shows the starting locations of all paths $\mathbf{Z}(t = 0)$ considered in the analyses that follow. The color scheme organizes the parcels by their position at the starting time. The color groups these by their proximity to the quiescent free surface at $t = 0$ and to the focusing position x_b at time $t = t_b$. Throughout this work we will connote the numerically-generated outcomes as *data*.

3. Transport Due to Breaking Monochromatic Progressive Waves

The Lagrangian velocity will be denoted by $\mathbf{U}(t) = \dot{\mathbf{Z}} = (U(t), W(t))$. The Stokes drift velocity is the lowest-order estimate of the mean Lagrangian velocity due to time periodic irrotational infinitesimal waves. For progressive waves of amplitude a_c , the Stokes drift is constant and proportional to a_c^2 (see Longuet-Higgins (1953)). In Restrepo (2007) this result was extended to include a stochastic velocity. The Eulerian velocity is decomposed as $\mathbf{q}(x, z, t) = \mathbf{q}^D(x, z, t) + \epsilon \mathbf{u}^w(x, z, t) + \epsilon^2 \mathbf{q}^C(x, z, t, X, T)$, where \mathbf{q}^D is a zero-mean velocity associated with unresolved stochastic sub-wave velocity contributions, \mathbf{u}^w is the irrotational or wave component of the velocity, whilst \mathbf{q}^C represents the rotational component, possibly including an imposed current \mathbf{v}^C as well as the velocity associated with transport due to waves and the residual flow due to breaking waves. This decomposition is based upon the assumption that wave orbital velocities are larger than currents (see McWilliams & Restrepo (1999) and Restrepo *et al.* 2011), and diffusive scale velocities, larger than wave orbital velocities. The stochastic component is a parametrization of unresolved processes. We will adopt a Wiener process to model this velocity (clearly, an ad-hoc representation that can elicit a number of objections, the least of which is that it is incompressible only in the mean). Associated with the above velocity decomposition, the parcel path decomposes as $\mathbf{Z} = \mathbf{Z}_0 + \epsilon \mathbf{Z}_1 + \epsilon^2 \mathbf{Z}_2 + \dots$. We use the operator $\langle \cdot \rangle$ to denote *ensemble average*, which in this case means expectation with respect to the stochastic component of \mathbf{q} , a Wiener noise process $W(t)$ satisfying $\langle W(t) \rangle = 0$, and $\langle W(t)W(t') \rangle = t D\delta_{t,t'}$ and affecting \mathbf{q} at the fastest time scales. Further, for some $f(t)$, \bar{f} denotes the average of f over the period $T_c = 1/\nu_c$. The critical observation in the

Longuet-Higgins (1953) analysis is that, in the case of a monochromatic wave component, say $\mathbf{u}^w(x, z, t) = -\nabla \frac{a_c \omega_c}{k_c} \frac{\cosh(k_c(z+h))}{\cosh(k_c h)} \cos(k_c(x - x_b) - \omega_c t)$, the compounded average $\langle \cdot \rangle$ of the lowest order Lagrangian and Eulerian velocities vanish. Hence

$$\langle d\mathbf{Z}_0 \rangle = \langle \sqrt{2D} d\mathbf{w}_t \rangle = 0, \quad (3.1)$$

$$\langle d\mathbf{Z}_1 \rangle = \langle \mathbf{u}^w(\mathbf{Z}_0, t) dt \rangle = 0, \quad (3.2)$$

$$\langle d\mathbf{Z}_2 \rangle = \mathbf{v}^C dt + \mathbf{u}^{St} dt, \quad (3.3)$$

where $d\mathbf{w}_t := (dW_t, 0)$. The third equation in (3.3) has the imposed current (if present) as well as the Stokes drift velocity. The Stokes drift $\mathbf{u}^{St} = (u_c^{St}, 0)$ can be obtained by computing

$$u_c^{St} = \left\langle \int_0^t \mathbf{u}^w(\mathbf{Z}_0, s) ds \cdot \nabla \mathbf{u}^w(\mathbf{Z}_0, t) \right\rangle,$$

where $\mathbf{Z}_0 = \mathbf{Z}_0(0) + \sqrt{2D} \mathbf{w}_t$. For progressive monochromatic shallow-water waves, the steady Stokes drift velocity is

$$u_c^{St} = \frac{S_c^2 c_p}{2} \mathcal{D} \cosh^2[k_c(z+h)] \operatorname{csch}(2k_c h), \quad (3.4)$$

with $S_c = k_c a_c$, $c_p = \omega_c / k_c$ is the phase speed, and $\mathcal{D} = \frac{1}{1+\Delta}$, where $\Delta = \frac{k_c^4 D^2}{\omega_c^2}$. The Stokes drift velocity is proportional to a_c^2 via S_c^2 . Note that the stochastic term leads to an increase in wave dispersion. It also leads to a suppression of wave-generated transport (see Restrepo (2007)). \mathcal{D} is 1 when the stochastic process is zero, leading to the familiar expression for the Stokes drift velocity under progressive monochromatic waves, obeying the shallow-water dispersion relation. Condition (3.2) holds exactly for monochromatic waves and holds as well for random-phase, stationary linear waves (see Huang (1971)). It does not hold for the transient from which our data was collected.

4. Transport due to Transient Waves

In the analysis of the data the *mean horizontal displacement* is defined as $\langle X(T_f) - X(0) \rangle$. In this context, the ensemble average of a quantity is estimated as the average of such quantity over all paths with initial location within the rectangle of black points in Figure 1. The assumption here is that the uncertainty modeled as a stochastic component in \mathbf{q} , translates into the data as uncertainty over the parcel paths initial condition $\mathbf{Z}(0)$. We also define *transport* as the mean horizontal velocity $\frac{\langle X(T_f) - X(0) \rangle}{T_f}$ over the whole simulation.

In what follows we enumerate essential aspects of the kinematics of the transport. These are used to later propose a model for the same. For transient waves, meaning for waves for which (3.2) does not hold over the time of interest, (3.1)-(3.3) does not apply and the Stokes drift, as defined narrowly above, makes no sense. The average transport needs to be obtained by averaging (2.2). If we set $\mathbf{q} \approx \mathbf{u}^w$ given by (2.1), we find that for parcels that are initially at the sea surface, When S is small (3.2) is approximately satisfied. For example, for $S = 0.16$, $\bar{U}(t) \approx 10^{-6}$. Hence (3.1)-(3.3) holds, approximately, and the Stokes drift is a good approximation of the average transport and hence proportional to S^2 . For $S = 0.32$, $\bar{U}(t) \approx 10^{-3}$; the transport is proportional to the amplitude of \mathbf{u}^w (i.e., to S) and is given by the average of (2.2). Figure 2 depicts the mean transport and the Stokes drift velocity as a function of depth for two values of S . Note that for large S , the

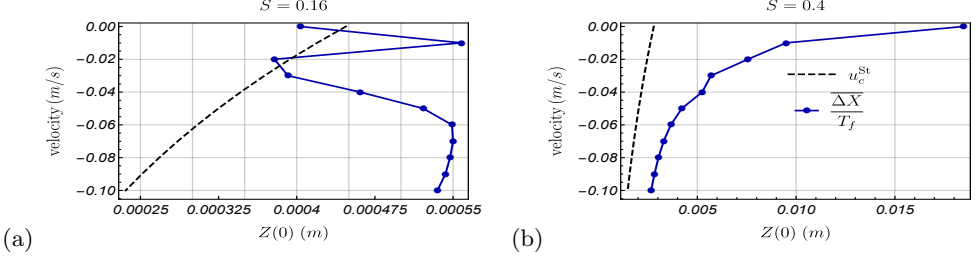


FIGURE 2. Mean horizontal transport as a function of depth, compared with the Stokes drift (dashed) for the cases (a) $S = 0.16$ and (b) $S = 0.4$, a breaking case. $T_f = 35$ s and the mean is taken over all paths with same initial depth. The Stokes drift velocity u_c^{St} is computed using (3.4) with $\mathcal{D} = 1$. (Note horizontal scales).

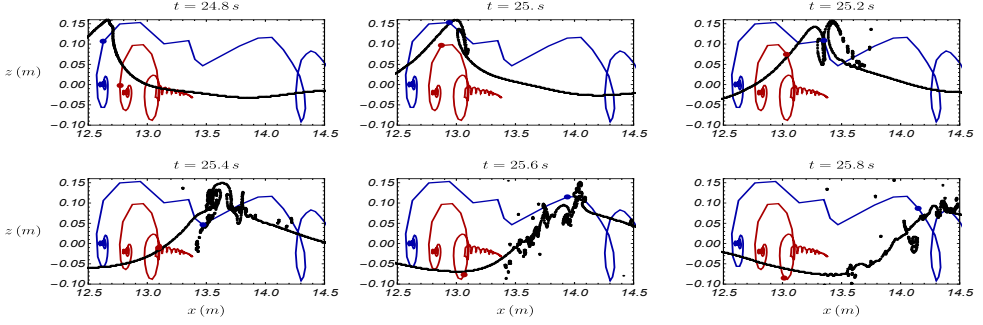


FIGURE 3. Lagrangian parcel path histories. $S = 0.4$, The breaking free surface is shown in black. The smoother path (red) that follows an elliptical path punctuated by a large displacement is typical of the overwhelming parcel paths. The more complex (blue) path is of the type we denote as a *rider* parcel path.

transport can be three times larger in the red region close to the surface of Figure 1. For small S , the parcel paths in most of the water column are the familiar-looking paths of monochromatic waves and transport is much better approximated by u_c^{St} . Figure 3 shows a couple of parcel paths for large S , *i.e.*, highly transient waves. The black line demarcates the (breaking) free surface. The blue path corresponds to a rider parcel (see Pizzo (2017)). These parcels spend a considerable amount of time on the free surface, resulting in a complex displacement history that is sensitive to the numerical resolution of the calculation. Their transport may be large, but they are also highly exceptional, as evidenced by Figure 4: they originate near x_b in the thin layer near the free surface denoted in red in Figure 1. The red path in Figure 3 is far more typical of the large S flows. The large excursion coincides with the wave passing overhead. As a function of depth, the red paths scale proportional to $\exp(kz)$.

If S is sufficiently large (larger than 0.3 for our data) wave breaking can occur and vorticity is generated in the flow and found to be confined to a very thin layer close to the sea surface. This vorticity lingers after the wave passes. Wave breaking enhances dispersion, regardless of the manner in which the waves break, but it is the ensuing vorticity that enhances transport. Figure 5 features several parcel paths for the $S = 0.4$ (breaking) case in different regions within the tank. Paths in the two lower rows are taken from the area highlighted in black in Figure 1 and are very typical of the paths under large unbreaking as well as breaking waves. In red we highlight the portion of the parcel flight that coincides with the wave passing overhead. Clearly, it is this large amplitude

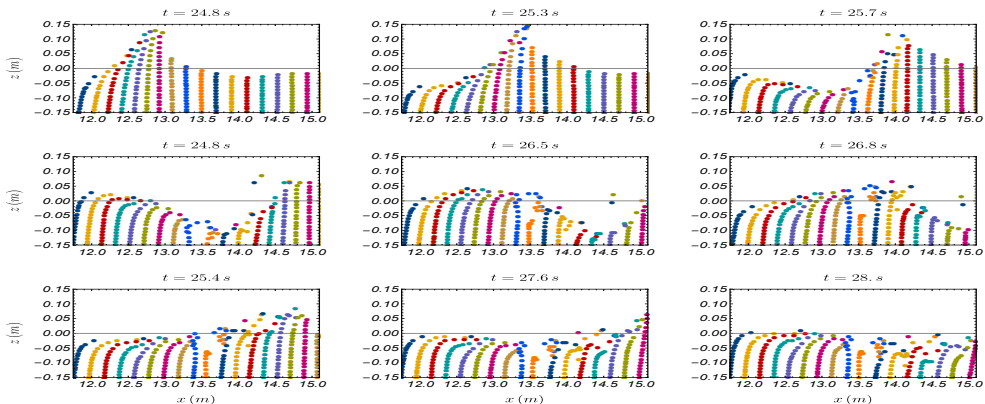


FIGURE 4. Evolution of parcel paths. $S = 0.4$. Transport is evidenced by irreversible forward displacement of the parcels. Complex-motion displacements are found to be confined to a very thin layer close to the free surface.

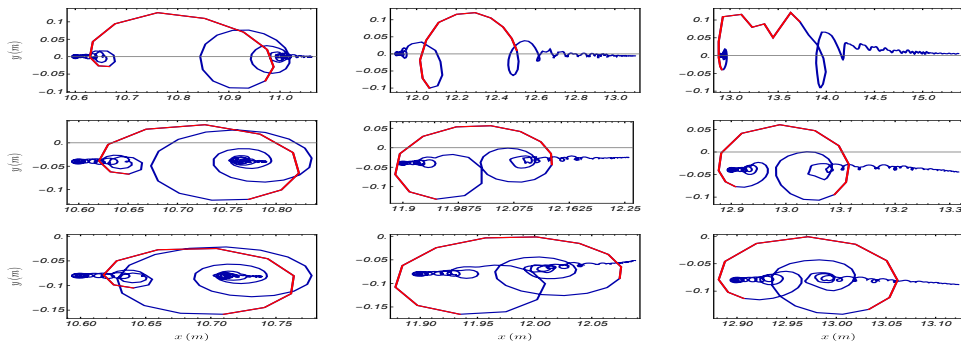


FIGURE 5. Lagrangian parcel path histories corresponding to different initial locations. The wave slope $S = 0.4$. Highlighted in red is the portion of the path when the crest of the wave passes overhead.

displacement and the residual motion after the wave passage that largely accounts for the transport. The lingering transport is marked when vorticity generation is present: wave momentum is transferred to the mean flow. For large amplitude the transport is proportional to S .

A time series of the horizontal component of the velocity, following one of the parcels is shown in the left panel of Figure 5. The right panel of Figure 6 depicts the horizontal velocity obtained from solving $\dot{\mathbf{Z}} = \mathbf{u}^w(\mathbf{Z}(t))$ with \mathbf{u}^w given by the linear field in (2.1), and initial conditions close to the surface. This equation forms the basis for the transport model to be presented later on. We note the qualitative similarity of the velocities in the two panels. Apparently, surface breaking, the generation of vorticity/dissipation inherent in the Navier-Stokes solution has a significant effect on the amplitude of the parcel path. Nevertheless, this comparison suggests that the linear field captures and explains a great deal of the transport. However, the amplitude of the transport would be overestimated by \mathbf{u}^w and thus we will propose a simple parametric dissipation correction, $\dot{\mathbf{Z}} = e^{-\beta t} \mathbf{u}^w(\mathbf{Z}(t))$ for some β to be determined from the data.

Figure 7 shows the time dependent mean and variance of the (horizontal) displacement, estimated from data. Large horizontal displacement are caused by large and highly transient amplitude waves. On the right we present the horizontal displacement variance.

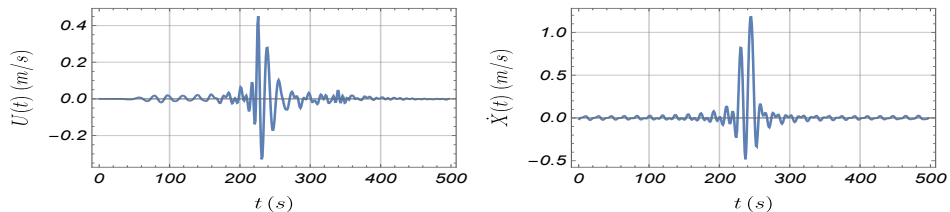


FIGURE 6. Left panel: horizontal Lagrangian velocity of a parcel with $\mathbf{Z}(0) = (10.6, -0.07)$ in the case $S = 0.4$. Right panel: horizontal Lagrangian velocity obtained by numerically solving $\dot{\mathbf{Z}} = \mathbf{u}^w(\mathbf{Z}(t))$ with \mathbf{u}^w given by (2.1). Note the difference in vertical scale. The spectrum of the forcing boundary condition creates a transient velocity everywhere in the tank.

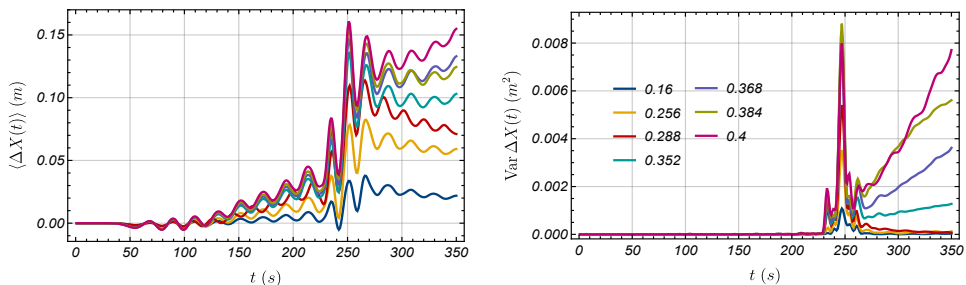


FIGURE 7. Mean (left) and variance (right) of the horizontal displacement $\Delta X(t) = X(t) - X(0)$. Averages are taken over the trajectories starting in points marked as black in Figure 1. The breaking cases correspond to $S > 0.29$ in this figure.

Before the wave passes overhead, the variance is nearly zero. Once the wave passes overhead, there is an injection of variance. For non-breaking cases, the variance reverts back to nearly zero, after the wave passes. However, this is not the case for breaking cases: the variance grows linearly, in fact. Wave breaking generates variability in the horizontal transport, coinciding with increased vorticity.

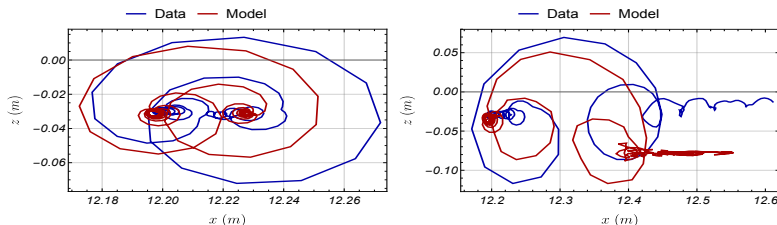
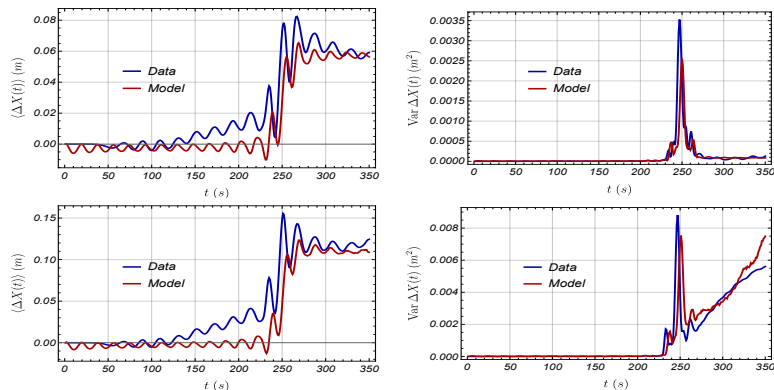
5. The Stochastic Model

The goal in this section is to propose a model for the transport due to transient progressive waves, including breaking waves. The model will apply for all values of S , regardless of whether $\overline{\mathbf{Z}}_1$ is small or otherwise. A model, consistent with the observations made in Section 4, is

$$\langle d\mathbf{Z} \rangle = \mathbf{v}^C dt + \langle e^{-\beta t} \mathbf{u}^w(\mathbf{Z}, t) dt + \sqrt{2D(t - t_b)} d\mathbf{w}_t \rangle. \quad (5.1)$$

The first term is zero in the data, but otherwise, would represent an imposed current. The model has two fitting parameters: the dissipation rate β and the molecular diffusion $D(t) = D_b \Theta(t - t_b)$, where $\Theta(t)$ is the Heaviside function, and D_b is a constant. The parameters β and D_b were estimated from data: we used the data to estimate the ensemble average $\langle X(T_f) - X(0) \rangle$ and then solved $d\tilde{\mathbf{Z}} = e^{-\beta t} \mathbf{u}^w(\tilde{\mathbf{Z}}, t) dt$ for the same initial locations, and numerically estimated the value of β such that $\langle \tilde{X}(T_f) - \tilde{X}(0) \rangle$ gave the best approximation to the average from the data. The value of D_b was estimated following the same fitting methodology using instead the second moment $\langle (X(T_f) - X(0))^2 \rangle$. The fitting results are shown in Table 1. Figure 8 compares data to paths from a single realization of the model in two contrasting cases: a large amplitude, non breaking case, $S = 0.26$ in (a), and a breaking case, $S = 0.4$ in (b). The data and the model outcome are

S	0.16	0.26	0.29	0.35	0.37	0.38	0.4
β (1/s)	0.0176	0.0195	0.0211	0.0221	0.0213	0.0219	0.0217
D_b (m ² /s)	0.0	0.0	0.0	0.00005	0.00014	0.00025	0.0003

TABLE 1. Estimated values of parameters β, D_b in (5.1)FIGURE 8. Comparison of data (approximations to (2.2)) and model (5.1) parcel paths, for $S = 0.26$ (left panel) and $S = 0.4$ (right panel). $\mathbf{Z}(0) = (12.2, -0.3)\text{m}$ in both cases.FIGURE 9. (Left) Ensemble mean of the horizontal displacement $\Delta X(t) = X(t_f) - X(0)$, and (Right) its variance as a function of time. Plots on top have $S = 0.256$ (non-breaking), and $S = 0.4$ for those in the bottom. Averages are taken over the trajectories starting in points marked as black in Figure 1.

similar qualitatively, and close quantitatively. For small S , the agreement between model and data is even better. Figure 9 compares ensemble displacement and variance of the data and model runs for $S = 0.26$ and $S = 0.4$ cases. The ensembles encompass data and model outcomes for all of the points marked as black in Figure 1. The only element giving structure to the model is what we call the linear velocity field \mathbf{u}^w . Figure 10 displays comparisons of data and model outcomes of the mean horizontal displacement and its variance, as a function of the slope S . There is good agreement between model and data, for a wide range of S .

6. Summary

We investigated the mean transport due to a progressive wave packet. The wave packet was produced by a boundary-driven Navier-Stokes solver capable of resolving the free surface. The velocity boundary condition has a parameter S which is proportional to the wave amplitude which controlled the overall amplitude of the waves as well as the

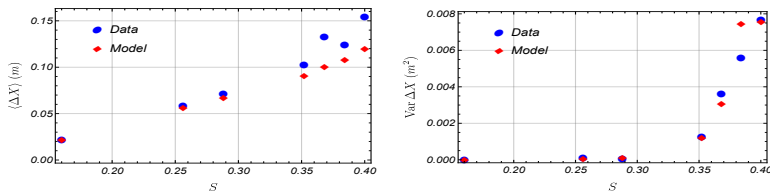


FIGURE 10. Comparisons of the mean horizontal displacement $\Delta X(t) = X(t_f) - X(0)$ (left), and variance (right), as a function of slope S . Averages are taken over the trajectories starting in positions marked as black in Figure 1.

transient character of the waves. For sufficiently large S wave breaking took place. The transport was analyzed by examining ensembles of numerically-generated Lagrangian parcel paths. When compared to the steady progressive wave case, in which transport is captured by the Stokes drift, transient wave packets can produce significantly more transport and dispersion. This was borne out by the data when S was large. Namely, the mean transport was proportional to the wave amplitude, and hence to S . When S was small, the mean transport is numerically closer to S^2 , as it would be if the waves were steady progressive waves. Mean transport varied smoothly with S and the explanation for this transition in magnitude rests upon the averaging: when S is small the wave average of the forcing is nearly zero, because the flow is not as transient, and thus the Stokes drift is an approximation of the resulting mean transport. For large S , on the other hand, the average wave forcing is significant and thus the Eulerian and Lagrangian means differ at all orders. When S is sufficiently large, the waves break. The transport generated in this case is still proportional to S but it is smaller than one would estimate had the wave not break. Vorticity starts appearing as S increases and it is very prominent in the breaking cases, yet confined to a layer of size proportional to the wave amplitude. Wave momentum transfers to the mean flow. During the breaking event parcels exhibit strong intermittent dispersion, but the breaking makes this dispersion persist and be of significance after the breaking event.

The same data we considered here was examined in DPM17. Their key conclusion is that mean transport is proportional to S for breaking waves and to S^2 when waves do not. They intimate a phase transition in transport that corresponds to the appearance of breaking waves (see their Figure 8). Clearly, our result is consistent with theirs, for large S . However, our other findings do not agree with the rest of their conclusions. Their conclusions are based upon the application of an analysis of parcel paths in Pizzo (2017)) of the Jones equation for surface Lagrangian velocities. This equation does not apply to rotational flows and/or breaking waves and they do not suggest then how it could be used to study the breaking wave cases. Nevertheless it does apply when S is very small and it would suggest that the peak transport velocity U is proportional to S . However, only after carefully averaging would they had obtained that the mean transport is proportional to S^2 for small S .

Another key finding of our work is that important aspects of the parcel velocity could be explained by \mathbf{u}^w (2.1). That is, by approximating $\mathbf{q}(\mathbf{Z}, t) \approx \mathbf{u}^w(\mathbf{Z}, t)$ in (2.2). For small S and for parcels far from the sea surface the approximation is even quantitatively close. The surprise is that, for non-breaking but large S cases, the approximation remains qualitatively similar when compared to the data, though no longer close quantitatively. Better quantitative comparisons are obtained when we multiply the velocity by an empirical dissipation term. The simplicity of this dissipation term might suggest that a more physically-motivated alternative could be proposed. For breaking waves vorticity in

the wave boundary layer. As a function of S , vorticity appears before S is large enough to make the waves break. However, for breaking waves, the vorticity persists in the wave boundary layer after the break and hence there is a momentum exchange between the irrotational part of the flow (the waves) and the mean field (the currents). These observations form the basis for a simple parametric stochastic mean transport model. This equation compares favorably for small S and for large S . Our model accommodates the effect of wave breaking on the mean transport and on enhancing dispersion, while at the same time introducing irrotationality due to the generation of vorticity generation. The stochastic aspect of the model is clearly too crude but at least argues that a stochastic modeling approach might be useful in capturing the effect of wave breaking on mean transport and dispersion.

By means of an exemplary flow we suggest here that transient wave transport and dispersion is significant, at the wave scale and beyond. Proposals on how Langmuir turbulence, for example, is modified to include wave breaking events appear in Sullivan *et al.* 2007, Restrepo *et al.* (2011). The same problem framework lends itself to investigate the impact of wave-induced transport and dispersion under transient conditions.

Acknowledgements: We thank L. Deike and K. Melville for sharing their data. We also thank James C. McWilliams for stimulating discussions and for suggesting improvements to the manuscript. This work was supported through a grant by the National Science Foundation, NSF OCE1434198. JMR wishes to thank the Kavli Institute of Theoretical Physics at the University of California, Santa Barbara. The KITP is supported in part by the National Science Foundation under Grant No. NSF PHY-1748958.

REFERENCES

- BURCHARD, H. 2001 Simulating the wave-enhanced layer under breaking surface waves with two-equation turbulence models. *Journal of Physical Oceanography* **31**, 3133–3145.
- DEIKE, L., PIZZO, N. & MELVILLE, W. K. 2017 Lagrangian transport by breaking surface waves. *Journal of Fluid Mechanics* **829**, 364–391.
- HUANG, NORDEN E. 1971 Derivation of stokes drift for a deep-water random gravity wave field. *Deep-sea research* **18**, 255–259.
- LONGUET-HIGGINS, M. 1953 Mass transport under waves. *Philosophical Transactions of the Royal Society A* **245**.
- MCWILLIAMS, J. C. & RESTREPO, J. M. 1999 The wave-driven ocean circulation. *Journal of Physical Oceanography* **29**, 2523–2540.
- MCWILLIAMS, J. C., SULLIVAN, P. P. & MOENG, C.-H. 1997 Langmuir turbulence in the ocean. *Journal of Fluid Mechanics* **334**, 1–30.
- MELVILLE, W. K. 1996 The role of surface-wave breaking in air-sea interaction. *Annual Review of Fluid Mechanics* **28**, 279–321.
- PIZZO, N. 2017 Surfing surface gravity waves. *Journal of Fluid Mechanics* **823**, 316–328.
- POPINET, S. 2009 An accurate adaptive solver for surface-tension-driven interfacial flows. *Journal of Computational Physics* **228**, 5838–5866.
- RESTREPO, J. M. 2007 Wave breaking dissipation in the wave-driven ocean circulation. *Journal of Physical Oceanography* **37**, 1749–1763.
- RESTREPO, J. M., RAMÍREZ, J. M., MCWILLIAMS, J. C. & BANNER, M. 2011 Multiscale momentum flux and diffusion due to whitecapping in wave-current interactions. *Journal of Physical Oceanography* **41**, 837–856.
- SULLIVAN, PETER P. & MCWILLIAMS, JAMES C. 2010 Dynamics of winds and currents coupled to surface waves. *Annual Review of Fluid Mechanics* **42**, 19–42.
- SULLIVAN, P. P., MCWILLIAMS, J. C. & MELVILLE, W. K. 2007 Surface gravity wave effects in the oceanic boundary layer: large-eddy simulation with vortex force and stochastic breakers. *Journal of Fluid Mechanics* **593**, 405–452.